European Drag Reduction and Flow Control Meeting – EDRFCM 2015
March 23–26, 2015, Cambridge, UK

COMBINATION OF WALL TRANSPIRATION AND SPINNING RINGS FOR TURBULENT DRAG REDUCTION

P. Ricco, S. Khosh Aghdam, M. Seddighi
Department of Mechanical Engineering, University of Sheffield, S1 3JD, Sheffield, UK

Direct numerical simulations (DNS) of a turbulent channel flow at a friction Reynolds number $Re_{\tau_0} = u^*_{\tau_0} h^*/\nu^* = 180$, where $u^*_{\tau_0}$ is the friction velocity in the uncontrolled case, h^* is the channel half-height and ν^* is the kinematic viscosity of the fluid, have been performed to study an active control technique in which steadily rotating flush-mounted of either discs [5] (RH13) or rings are combined with the opposition control method [1]. Wall transpiration is applied with a controlled wall velocity which has the same amplitude but opposite sign to that of the optimum detection plane at $y^+ \approx 15$, aiming at suppressing the near-wall quasi-streamwise vortices. Various configurations are examined using the out-of-phase v (wall-normal) and w (spanwise) control, and the steadily rotating discs and rings.

The Incompact3d DNS code [3, 4] was used for the simulations. The disc flow domain is sketched in figure 1. For the discs, two parameters are relevant, i.e. the disc tip velocity (W) and the disc diameter (D). The instantaneous flow $\mathbf{u}$ can be decomposed into a mean flow $\mathbf{u}_m$, disc/ring flow $\mathbf{u}_d$, and the turbulent contribution $\mathbf{u}_t$: $\mathbf{u} = \mathbf{u}_m + \mathbf{u}_d + \mathbf{u}_t$, where $\mathbf{u}_d = \overline{\mathbf{u}} - \mathbf{u}_m$ (the overbar indicates the time average).

Several combinations of the two control strategies have been studied to obtain as high drag reduction values as possible. The original disc configuration investigated in RH13 was modified by substituting the central part of the discs with stationary wall, thereby forcing the flow through spinning annuli. Opposition-control wall transpiration was enforced on the stationary wall portions, i.e. between the rings and in the core of the rings. Figure 2 shows a contour of the instantaneous velocity in the spinning-ring case with opposition control.

The results are shown in Table 1 where the opposition control strategy is based on the wall-normal velocity.

The drag reduction, the net energy saving and the changes in the turbulence structures have been compared with those cases for which the two control methods are applied separately. When the optimum rotating disc case [5] is used together with the out-of-phase opposition control of wall-normal velocity, an additional drag reduction of 5% is achieved. When the spinning rings are combined with wall transpiration, the maximum drag reduction is 31%, i.e. larger than the values obtained by the two methods separately.

The net power saved is computed using $\mathcal{P}_{\rm net} = \mathcal{R} - (\mathcal{P}_{\rm spent,d} + \mathcal{P}_{\rm spent,opp})$, where $\mathcal{R}$ is the power saved thanks to drag reduction, $\mathcal{P}_{\rm spent,d}$ is the power spent to activate the discs and $\mathcal{P}_{\rm spent,opp}$ is the power spent to enforce the wall transpiration. For the last rings configuration in Table 1, $\mathcal{P}_{\rm net} = 6\%$ for the uncontrolled flow, while combined with the opposition control technique, this quantity reaches 13% which is higher than the optimum found by the discs alone.

The intensity of the main turbulence statistics is reduced, as shown in figure 3. The Fukagata identity (FIK) [2], $C_f = C_{f,\rm laminar} + (12/Re_b)\int (1-y)\langle -uv\rangle \, dy$ (where Re_b is the bulk Reynolds number and the operator $<>$ denotes time and space averaged along the streamwise and spanwise directions), is also employed. Figure 4 shows how the turbulent part of the weighted shear-stress is reduced by the control, thereby reducing the skin-friction coefficient. For a general control problem, the FIK identity is developed (lower-wall):

$$C_{f,\rm lw} = -12 \int_0^2 (2-y)\left[u_m v_m + u_d v_d + \langle \overline{u_t v_t}\rangle\right] \mathrm{d}y$$
$$+24\left[u_m(0)v_m(0) + u_d(0)v_d(0) + \langle \overline{u_t(0)v_t(0)}\rangle\right]$$
$$+16A_0 + \frac{12}{Re_b}\left[1 - 2u_m(0)\right] \qquad (1)$$

A similar expression is derived for the upper-wall. A_0 is a constant due to the wall forcing.

Figure 5 shows isosurfaces of the spinning-ring flow. The intensity of the tube shaped structures, which appear between discs, is reduced when opposition control is applied.

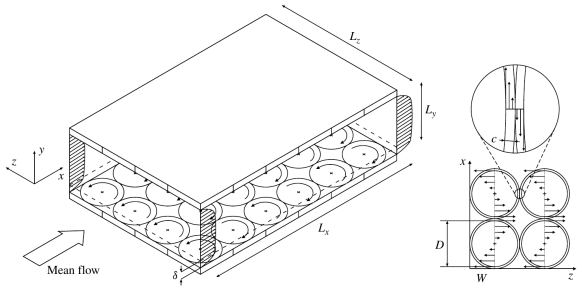

Figure 1: Flow configuration with steady rotating discs. The buffer region (with width c) is assigned to model the gap between discs and stationary wall.

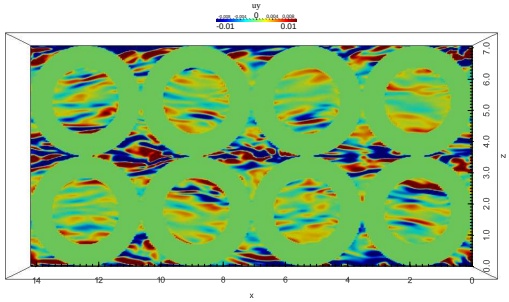

Figure 2: Instantaneous wall-normal velocity $v(x, y = 0, z)$. The green areas represent the location of the ring actuators.

case	L_x	L_z	W^{+0}	D^{+0}	$\mathcal{R}(\%)$
discs	6.79π	2.26π	9	640	18.8
discs + OC	6.79π	2.26π	9	640	20.5
rings	4.53π	2.26π	9	640	19.8
rings + OC	4.53π	2.26π	9	640	26.8
rings	6.79π	3.39π	6	960	18.1
rings + OC	6.79π	3.39π	6	960	26.4
discs	6.79π	3.39π	9	960	22.8
discs + OC	6.79π	3.39π	9	960	26.2
rings	6.79π	3.39π	9	960	**24**
rings + OC	6.79π	3.39π	9	960	**31**

Table 1: Discs and rings configurations tested with and without opposition control based on out-of-phase wall-normal velocity (OC).

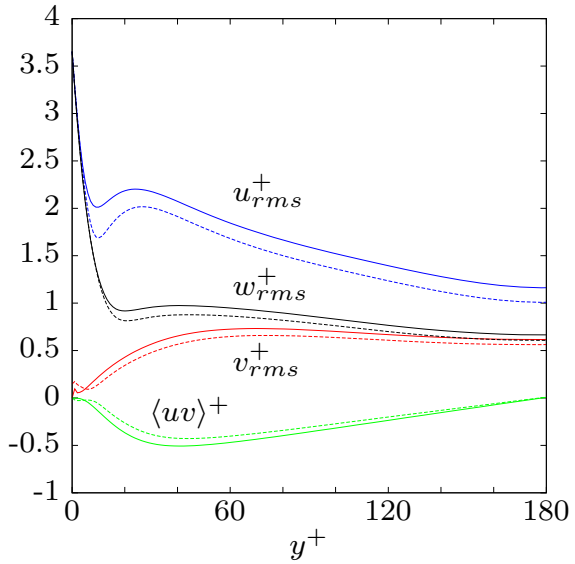

Figure 3: Statistics for the rings. Solid lines: rings without control, dashed lines: rings with v-control. Normalisation is done with respect to the uncontrolled case.

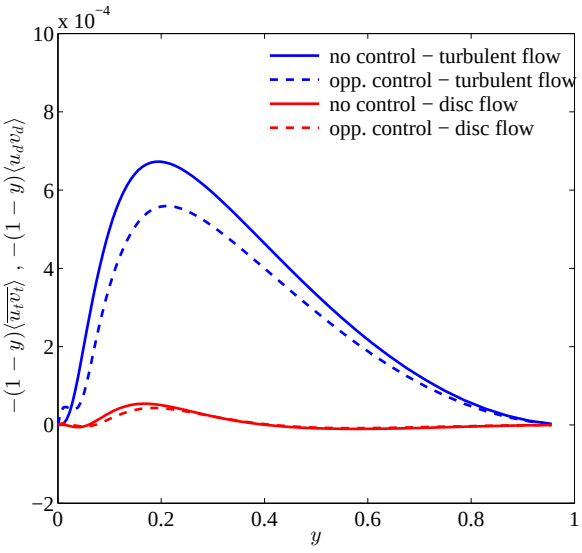

Figure 4: Weighted Reynolds stress terms.

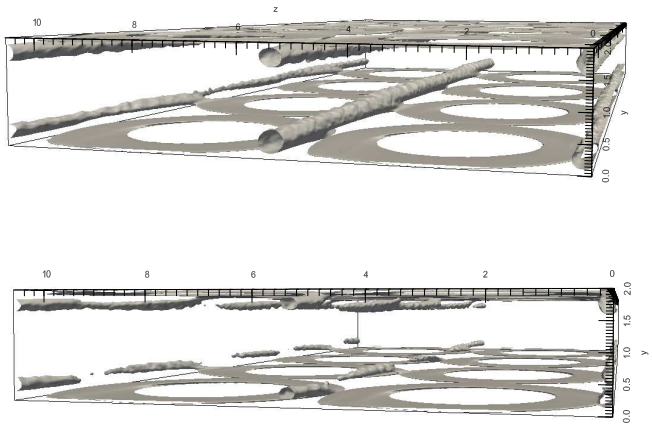

Figure 5: Isosurface representation for rings ($\sqrt{u_d^2+v_d^2+w_d^2}=0.09$) without (top) and with opposition control (bottom). Tube-shaped patterns are present as in the uncontrolled case but they are damped.

REFERENCES

[1] H. Choi, P. Moin, and J. Kim. Active turbulence control for drag reduction in wall-bounded flows. *J. Fluid Mech.*, 262:75–110, 1994.

[2] K. Fukagata, K. Iwamoto, and N. Kasagi. Contribution of Reynolds stress distribution to the skin friction in wall-bounded flows. *Phys. Fluids*, 14:L73–L76, 2002.

[3] S. Laizet and E. Lamballais. High-order compact schemes for incompressible flows: A simple and efficient method with quasi-spectral accuracy. *J. Comp. Phys.*, 228(16):5989–6015, 2009.

[4] S. Laizet and N. Li. Incompact3d: A powerful tool to tackle turbulence problems with up to $O(10^5)$ computational cores. *Int. J. Num. Meth. Fluids*, 67:1735–1757, 2011.

[5] P. Ricco and S. Hahn. Turbulent drag reduction through rotating discs. *J. Fluid Mech.*, 722:267–290, 2013.